Prediction of giant tunneling magnetoresistance in $RuO_2/TiO_2/RuO_2$ (110) antiferromagnetic tunnel junctions

Yuan-Yuan Jiang,[1,2] Zi-An Wang,[1,2] Kartik Samanta,[3] Shu-Hui Zhang,[4] Rui-Chun Xiao,[5] W. J. Lu,[1] Y. P. Sun,[6,1,7] Evgeny Y. Tsymbal,[3,*] and Ding-Fu Shao[1,†]

[1]*Key Laboratory of Materials Physics, Institute of Solid State Physics, HFIPS, Chinese Academy of Sciences, Hefei 230031, China*
[2]*Science Island Branch of Graduate School, University of Science and Technology of China, Hefei 230026, China*
[3]*Department of Physics and Astronomy & Nebraska Center for Materials and Nanoscience, University of Nebraska, Lincoln, Nebraska 68588-0299, USA*
[4]*College of Mathematics and Physics, Beijing University of Chemical Technology, Beijing 100029, People's Republic of China*
[5]*Institute of Physical Science and Information Technology, Anhui University, Hefei 230601, China*
[6]*High Magnetic Field Laboratory, HFIPS, Chinese Academy of Sciences, Hefei 230031, China*
[7]*Collaborative Innovation Center of Microstructures, Nanjing University, Nanjing 210093, China*

(Received 5 September 2023; accepted 8 November 2023; published 27 November 2023)

Using first-principles quantum-transport calculations, we investigate spin-dependent electronic and transport properties of antiferromagnetic tunnel junctions (AFMTJs) that consist of (110)-oriented antiferromagnetic (AFM) metal RuO_2 electrodes and an insulating TiO_2 tunneling barrier. We predict the emergence of a giant tunneling magnetoresistance (TMR) effect in a wide energy window, a series of barrier layer thicknesses, and different interface terminations, indicating the robustness of this effect. We show that the predicted TMR cannot be explained in terms of the global transport spin-polarization of RuO_2 (110) but is well understood based on matching the momentum-dependent spin-polarized conduction channels of the two RuO_2 (110) electrodes. We predict oscillations of TMR with increasing barrier thickness, indicating a non-negligible contribution from the perfectly epitaxial interfaces. Our work helps the understanding of the physics of TMR in AFMTJs and aids in realizing efficient AFM spintronic devices.

DOI: 10.1103/PhysRevB.108.174439

I. INTRODUCTION

Spintronics utilizes a spin degree of freedom and magnetic order parameters as state variables to encode information [1]. The electrical readout of information in spintronic devices requires a strong transport response to the variation of the magnetic order parameters. A typical and widely used spintronic device is a magnetic tunnel junction (MTJ) that is composed of two ferromagnetic (FM) metal electrodes separated by a nonmagnetic insulating tunneling barrier [2–7]. In MTJs, low and high resistance states occur for parallel and antiparallel magnetization of the two electrodes, respectively. This effect, known as tunneling magnetoresistance (TMR), offers an ON/OFF ratio as high as a few hundred percent, sufficient for accurate readout. Due to TMR, MTJs can serve as building blocks of magnetic random-access memories (MRAMs) for data storage and processing [8].

The TMR effect in MTJs has been widely understood in terms of a spin-polarized tunneling current that is controlled by the relative magnetization orientation of the two FM electrodes. This mechanism is often empirically quantified by Julliere's formula, $\mathrm{TMR} = \frac{2p_1p_2}{1-p_1p_2}$, where p_i $(i = 1, 2)$ is the transport spin polarization of the ith FM electrode in a MTJ [2]. Based on this formula, a larger spin polarization of the electrodes favors a larger TMR. While Julliere's formula offers a qualitative explanation of TMR, in crystalline MTJs where the transverse wave vector is conserved in the tunneling process, a more accurate description should take into account symmetry matching of the incoming and outgoing Bloch states in the electrodes and evanescent states in the barrier [9]. In particular, matching the majority-spin Δ_1 band in the Fe (001) electrode to the Δ_1 evanescent state in the MgO (001) barrier layer is responsible for a large positive spin polarization and giant values of TMR predicted for crystalline Fe/MgO/Fe (001) MTJs [10,11]. These concepts seem to rule out using antiferromagnetic (AFM) metals as electrodes in MTJs due to the spin degeneracy, and hence $p_i = 0$ is expected for antiferromagnets with their zero net magnetization.

This understanding has been challenged by the recent theoretical [12–15] and experimental [16,17] demonstrations of a sizable TMR effect in AFM tunnel junctions (AFMTJs). AFMTJs represent tunnel junctions with two AFM electrodes, where the TMR effect occurs in response to a change of the relative orientation of the AFM order parameters, known as the Néel vectors. The TMR effect relies on the conservation of the transverse momentum in the process of tunneling that requires epitaxial AFMTJs with a well-defined crystalline texture propagating across the whole junction. The possibility of TMR in AFMTJs opens perspectives for employing antiferromagnets in MRAMs, making use of their advantages

*tsymbal@unl.edu
†dfshao@issp.ac.cn

of being robust against magnetic perturbations, not producing stray fields, and exhibiting ultrafast spin dynamics [18,19].

In our previous work [12], using first-principles quantum transport calculations, we have explored $RuO_2/TiO_2/RuO_2$ (001) AFMTJs. These AFMTJs employed RuO_2—a high-temperature AFM metal exhibiting a spin-split band structure [20,21]. We predicted that TMR in these AFMTJs was controlled by the matching of the spin-polarized conduction channels in the two RuO_2 (001) electrodes. As a result, a large TMR appeared in these AFMTJs, even in the presence of the globally spin-neutral currents. This implies that the net spin polarization of the electrodes is not essential for obtaining a large TMR in AFMTJs.

Recent theoretical predictions also show that the antiferromagnets with spin-split band structures, including the noncollinear antiferromagnets [22,23] and certain types of collinear antiferromagnets [24–28], dubbed altermagnets [29,30], are capable of supporting longitudinal spin-polarized currents [31]. For example, it has been predicted that the spin currents occur along the crystallographic directions different from (001) in RuO_2 [28]. Specifically, the presence of a spin-polarized longitudinal current with a large polarization p_i is expected to directly support TMR in the relevant AFMTJs, according to the conventional Julliere's picture. It would be interesting to explore the role of this contribution to the total TMR response associated with the spin-dependent Fermi surface of RuO_2.

To address this question, we consider an AFMTJ based on RuO_2 electrodes that are stacked in the (110) plane, where the crystallographic [110] direction of RuO_2 supports spin-polarized transport providing a "direct" contribution to TMR similar to a conventional MTJ. We perform first-principles quantum-transport calculations of TMR in $RuO_2/TiO_2/RuO_2$ (110) AFMTJs and find a giant effect for a series of TiO_2 barrier thicknesses. We argue that the predicted TMR effect cannot be explained by the conventional picture based on the globally spin-polarized current emitted by the RuO_2 (110) electrode but rather originates from the matching of the spin-polarized conduction channels in the two RuO_2 (110) electrodes. These results uncover the important physics of the TMR effect which may be useful for the practical realization of AFMTJs.

II. THEORETICAL METHODS

First-principles calculations are performed based on density functional theory (DFT) [32] as implemented in the Vienna *ab initio* simulation package (VASP) [33,34]. The pseudopotentials are described using the projector augmented wave (PAW) method [35], and the exchange-correlation functional is treated within the generalized gradient approximation (GGA) developed by Perdew, Burke, and Ernzerhof (PBE) [36]. In the calculations, the cutoff energy for the plane-wave expansion is set to 500 eV, and the k-point grid is set to $16 \times 16 \times 16$ to sample the irreducible Brillouin zone. The GGA + U [37,38] method with $U_{\text{eff}} = 2$ eV on Ru $4d$ orbitals and $U_{\text{eff}} = 5$ eV on Ti $3d$ orbitals is employed in the calculations for RuO_2 and TiO_2. The Fermi surfaces are calculated using the WANNIER90 code [39] with the maximally localized Wannier functions [40,41] and visualized by FermiSurfer [42].

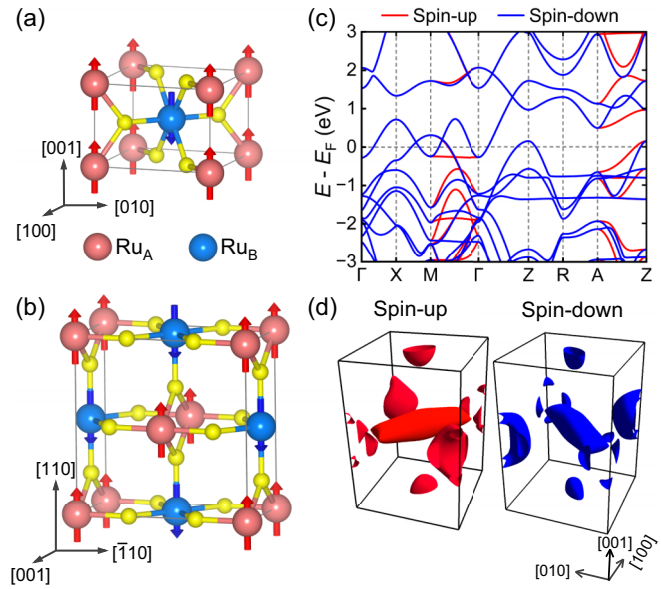

FIG. 1. (a) The atomic and magnetic structures of a RuO_2 unit cell. (b) The atomic and magnetic structures of a RuO_2 supercell stacked in the (110) plane. (c) The band structure of RuO_2. (d) The spin-up and spin-down Fermi surfaces of RuO_2.

Transport properties are calculated using the nonequilibrium Green's function formalism (the DFT+NEGF approach) [43,44], as implemented in QuantumATK, Synopsys QuantumATK [45] using the atomic structures relaxed by VASP. In QuantumATK, we set the cutoff energy of 100 Ry and use the nonrelativistic SG15 pseudopotentials [46], and k-point meshes of $12 \times 12 \times 12$ for bulk RuO_2 and TiO_2 and $11 \times 11 \times 101$ for $RuO_2/TiO_2/RuO_2$ (110) AFMTJ. The spin-polarized GGA+U [37,38] method with $U_{\text{eff}} = 1.2$ eV on Ru $4d$ orbitals and $U_{\text{eff}} = 5$ eV on Ti $3d$ orbitals is used in the calculations. These parameters have been well tested to ensure that the electronic structure around E_F calculated by QuantumATK is consistent with that calculated by VASP. Transmission functions are calculated using k-point meshes of 401×401 in the two-dimensional (2D) Brillouin zone of RuO_2 (110) and RuO_2 (110) based AFMTJs.

III. RESULTS AND DISCUSSION

The AFM metal RuO_2 [20] has a rutile structure with two spin sublattices Ru_A and Ru_B [Figs. 1(a) and 1(b)]. Its Néel vector is pointing along the [001] direction, and the Néel temperature is reported to be above 300 K [20]. RuO_2 can be considered as a C-type antiferromagnet with strong *intrasublattice* coupling along the [001] direction. As a result, a globally spin-neutral current along this direction is carried by the staggered Néel spin currents on the two magnetic sublattices, resulting in a giant TMR effect [12] and a fieldlike spin-transfer torque (STT) that enables deterministic switching of the RuO_2 (001) Néel vector [47]. The magnetic space group of RuO_2 is $P4'_2/mnm'$. It supports fully compensated antiferromagnetism with a spin-split electronic band

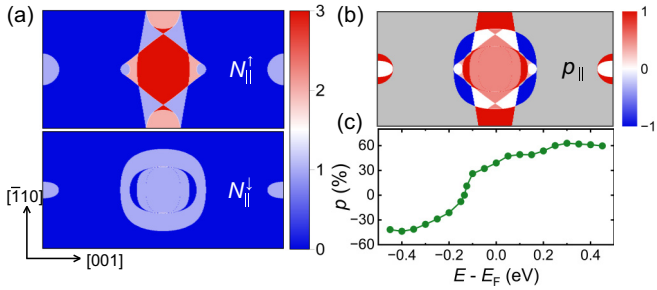

FIG. 2. (a) The conduction channels in the 2D Brillouin zone of RuO_2 (110) for spin up ($N_\parallel^\uparrow$) and spin down ($N_\parallel^\downarrow$) at the Fermi energy. (b) The spin polarization of conduction channels ($p_\parallel$) at the Fermi energy for RuO_2 (110), where the gray color indicates regions with $N_\parallel^\uparrow = N_\parallel^\downarrow = 0$. (c) The global transport spin polarization of RuO_2 (110) as a function of energy.

structure [21]. Figure 1(c) shows the calculated band structure of RuO_2, indicating a pronounced spin splitting along the high-symmetry Γ-M and Z-A directions. Figure 1(d) displays the associated spin-up and spin-down Fermi surfaces of RuO_2. They can be transformed to each other by a 90° rotation around the [001] direction. Such momentum-dependent spin splitting is responsible for various spin-dependent transport properties [31,48–52].

The spin-split Fermi surface of RuO_2 supports longitudinal spin-polarized currents along the [110] or [1̄10] directions [28]. This is evident from the calculated ballistic transmission of bulk RuO_2 along the [110] direction which reflects the number of conduction channels, i.e., the number of the propagating Bloch states in RuO_2 [110]. In the calculation, we used a supercell of RuO_2 along the [110] direction shown in Fig. 1(b). Figure 2(a) displays the number of conduction channels $N_\parallel^\uparrow$ ($N_\parallel^\downarrow$) contributed by the spin-up (spin-down) Fermi surface at different transverse wave vector $\vec{k}_\parallel$ in the 2D Brillouin zone of RuO_2 (110) [53]. We find a region of a finite $N_\parallel^\uparrow$ around the zone center, resulting in the maximum $N_\parallel^\uparrow = 3$. There are also some small pockets of $N_\parallel^\uparrow = 1$ at the left and right edges of the zone. The regions of a finite $N_\parallel^\downarrow$ have a smaller area located around the zone center and at the left and right edges of the zone. We find that $N_\parallel^\downarrow = 1$ in all these regions of the spin-down Fermi surface.

Figure 2(b) shows the $\vec{k}_\parallel$-dependent spin polarization that is defined as follows:

$$p_\parallel(\vec{k}_\parallel) = \frac{N_\parallel^\uparrow - N_\parallel^\downarrow}{N_\parallel^\uparrow + N_\parallel^\downarrow}. \quad (1)$$

The full spin polarization ($p_\parallel = \pm 100\%$) appears in the regions of a finite $N_\parallel^{\uparrow,\downarrow}$ with no overlap between spin-up and spin-down conduction channels. The region around the zone center exhibits a relatively small spin polarization [$p_\parallel = 50\%$ in the pink colored area and $p_\parallel = 0$ in the white colored area in Fig. 2(b)].

Figure 2(c) shows the calculated total transport spin polarization as a function of energy that is defined as follows:

$$p = \frac{\sum_{\vec{k}_\parallel} N_\parallel^\uparrow - N_\parallel^\downarrow}{\sum_{\vec{k}_\parallel} N_\parallel^\uparrow + N_\parallel^\downarrow}. \quad (2)$$

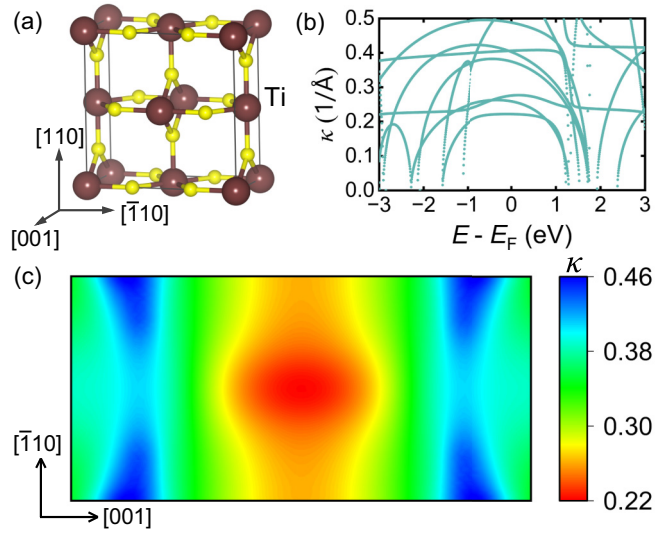

FIG. 3. (a) The atomic structures of a TiO_2 supercell stacked in the (110) plane. (b) The complex band structure of TiO_2 (110) at the Γ point. (c) The lowest decay rates of the evanescent states in TiO_2 (110) as a function of $\vec{k}_\parallel$ at the Fermi energy.

As expected [and in contrast to RuO_2 (001)], the total spin polarization is nonzero despite the antiferromagnetism of RuO_2. We find that $p = 39\%$ at the Fermi energy (E_F), which is comparable to the spin polarization of representative ferromagnetic metals such as Fe, Co, and Ni [54–56]. The spin polarization is enhanced with the increase of energy, reaching a maximum value of $p = 63\%$ at $E = 0.3$ eV, reduced at lower energy, and changes sign at around $E = -0.135$ eV.

Next, we consider a $RuO_2/TiO_2/RuO_2$ (110) AFMTJ where RuO_2 (110) serves as electrodes and TiO_2 (110) [Fig. 3(a)] as the barrier material. Due to the same rutile structure and similar lattice constants of bulk RuO_2 and TiO_2, such epitaxial AFMTJ is viable in practice. To characterize the evanescent states in bulk TiO_2 (110), we calculate the complex band structure at the Γ point [Fig. 3(b)] and the lowest decay rates of the evanescent states in TiO_2 (110) at the Fermi energy [Fig. 3(c)]. We find that TiO_2 (110) exhibits the smallest decay rates around the vertical midline of the 2D Brillouin zone. Figure 4(a) shows the atomic structure of a $RuO_2/TiO_2/RuO_2$ (110) heterostructure, including two TiO_2 monolayers in the

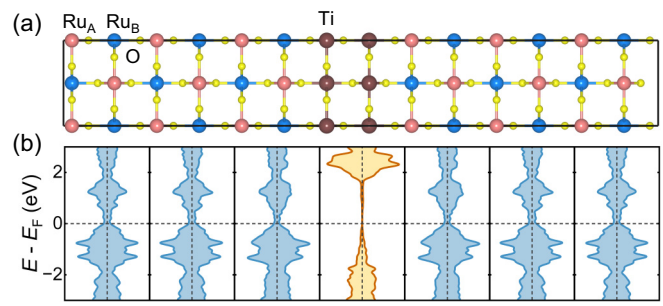

FIG. 4. (a), (b) The atomic structure (a) and layer-resolved density of states (DOS) (b) of the $RuO_2/TiO_2/RuO_2$ (110) heterostructure. Each DOS panel contains two MO_2 monolayers (M = Ru, Ti).

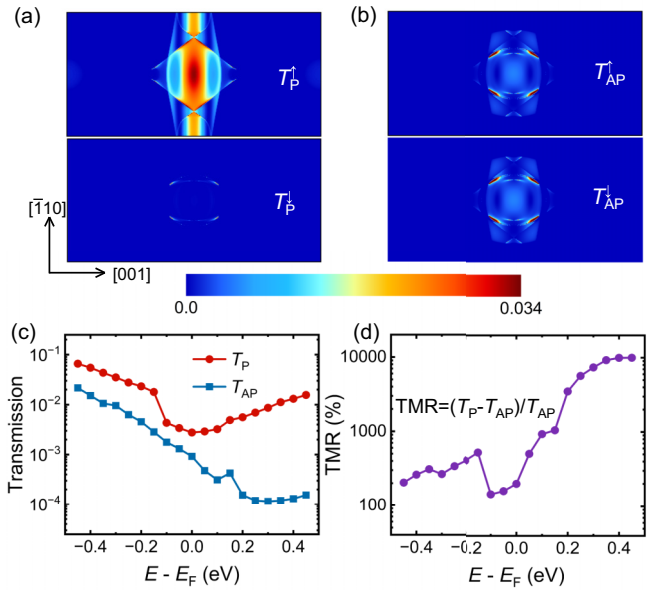

FIG. 5. The calculated $\vec{k}_{\parallel}$-resolved transmission in the 2D Brillouin zone for the AFMTJ in parallel (P) (a) and antiparallel (AP) (b) states. (c) The total transmission as a function of energy for the AFMTJ in the P state (red dots) and the AP state (blue dots). (d) TMR as a function of energy.

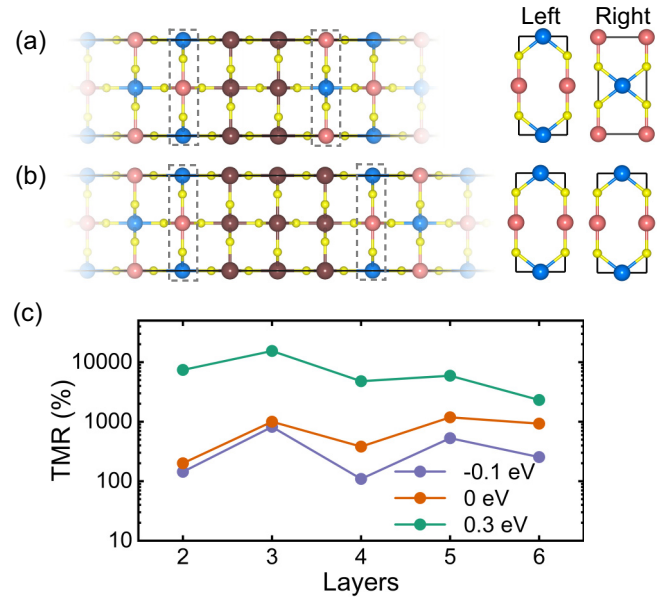

FIG. 6. The barrier and interface atomic structure for $RuO_2|TiO_2|RuO_2$ (110) AFMTJs with TiO_2 thickness of two layers (a) and three layers (b). (c) TMR as a function of the number of TiO_2 monolayers for different energies.

center and six RuO_2 monolayers on each side. As seen from the layer-resolved density of states (DOS) in Fig. 4(b), the Fermi energy lies in the middle of the band gap of TiO_2, while some nonvanishing local DOS in the band gap of the TiO_2 layer is due to the metal-induced gap states resulting from RuO_2 electrodes. As shown in the Supplemental Material [53], with the increasing TiO_2 layer thickness, the band gap opens wider thus sustaining the insulating character of TiO_2 and the tunneling transport regime in the AFMTJ.

The $RuO_2/TiO_2/RuO_2$ (110) heterostructure shown in Fig. 4(a) serves as the scattering region in an AFMTJ by connecting this region to two semi-infinite RuO_2 (110) electrodes. This geometry allows calculating electron transmission, as described in Sec. II. Figures 5(a) and 5(b) shows the calculated $\vec{k}_{\parallel}$-resolved transmission for the parallel (P) state of the AFMTJ, $T_P^{\sigma}(\vec{k}_{\parallel})$, and for the antiparallel (AP) state, $T_{AP}^{\sigma}(\vec{k}_{\parallel})$, where the $\sigma = \uparrow$ or $\downarrow$ is the spin index. We find that only conduction channels around the vertical midline in the 2D Brillouin zone contribute to the transmission. This is due to the evanescent states in TiO_2 having the lowest decay rates in this region [Fig. 3(c)] and thus being mostly supportive to electron transmission. For the P state, the distribution of $T_P^{\uparrow}(\vec{k}_{\parallel})$ qualitatively reflects that of $N_{\parallel}^{\uparrow}$ [compare the top panels in Figs. 2(a) and 5(a)], while $T_P^{\downarrow}(\vec{k}_{\parallel})$ is significantly suppressed [Fig. 5(a), bottom panel], indicating that spin-up electrons dominate in the tunneling process. On the other hand, for the AP state, $T_{AP}^{\sigma}(\vec{k}_{\parallel})$ vanishes at those $\vec{k}_{\parallel}$ where $|p_{\parallel}| = 100\%$ and is finite only at $\vec{k}_{\parallel}$ where $p_{\parallel}$ is small with the maximum of $T_{AP}^{\sigma}(\vec{k}_{\parallel})$ appearing at $\vec{k}_{\parallel}$ with $p_{\parallel} = 0$ [compare Figs. 2(b) and 5(b)]. These facts indicate the $T_P^{\sigma}(\vec{k}_{\parallel})$ and $T_{AP}^{\sigma}(\vec{k}_{\parallel})$ are largely controlled by the matching of the spin polarization $p_{\parallel}$ of the conduction channels of the two electrodes.

Figure 5(c) shows the total transmission as a function of energy for the $RuO_2/TiO_2/RuO_2$ (110) AFMTJ in the P state (T_P) and AP state (T_{AP}). The T_P is always greater than T_{AP}, leading to a positive TMR ratio $[(T_P - T_{AP})/T_{AP}]$ [Fig. 5(d)]. We find notable TMR = 200% at E_F, much larger than that predicted by Julliere's formula TMR $= \frac{2p_1p_2}{1-p_1p_2}$, using $p_1 = p_2 = 39\%$. Moreover, the maximum TMR at energies above E_F does not appear at $E = 0.3$ eV where p_1 and p_2 reach a maximum, and the TMR around $E = -0.135$ eV is still very large even though $p_1 = p_2 = 0$. These facts indicate that TMR cannot be described in terms of the total transport spin polarization, but requires knowledge of its distribution in the momentum space.

We note here that while we are using the concept of $\vec{k}_{\parallel}$-dependent spin polarization $p_{\parallel}(\vec{k}_{\parallel})$ to qualitatively analyze TMR in terms of the Fermi surface matching, this quantity can be used for the *quantitative* prediction of TMR. A more rigorous description requires using the interface transmission function and its spin polarization [57,58]. The latter takes into account not only the momentum- and spin-dependent Bloch states in the electrode, but also the evanescent states in the barrier as well as the transmission across the interface. The purpose of the present analysis is therefore just to emphasize the deficiency of the total spin polarization and the importance of the Fermi surface matching in the qualitative picture of TMR in AFMTJs based on spin-split antiferromagnets.

Next, we calculate TMR in $RuO_2/TiO_2/RuO_2$ (110) AFMTJs with larger thickness of the TiO_2 barrier. In the ideal crystalline AFMTJs, changing TiO_2 thickness alters the interface structure, as shown in Figs. 6(a) and 6(b). For all barrier

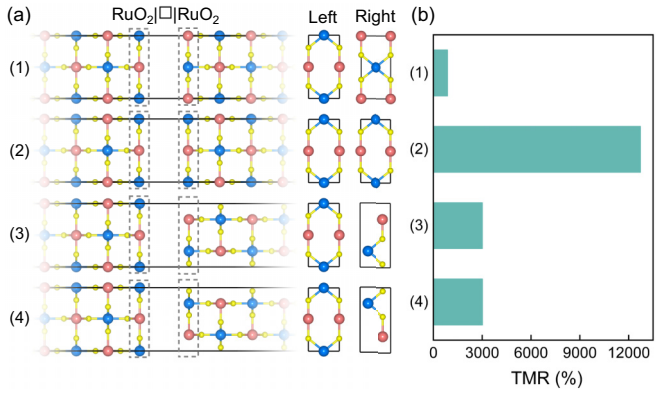

FIG. 7. (a) The supercells and interface atomic structures for $RuO_2|\square|RuO_2$ (110) AFMTJs. (b) The calculated TMR for the four AFMTJs in (a) at the Fermi energy.

thicknesses considered, we find a positive TMR. This indicates that the TMR mainly originates from the spin-polarized conduction channels of bulk RuO_2 (110). However, we find that TMR in AFMTJs with an odd number of TiO_2 monolayers is always larger than TMR in AFMTJs with an even number of TiO_2 monolayers, leading to an oscillation of TMR as a function of barrier thickness [Fig. 6(c)]. We attribute this phenomenon to the effect of interface. As shown in Fig. 6(a), for an AFMTJ with an even number of TiO_2 monolayers, the left and right interfacial RuO_2 monolayers are asymmetric and can be transformed to each other by a half-unit cell translation along the vertical direction. In this case, the P (AP) state of the AFMTJ has AP (P) interfacial magnetic moments in the horizontal Ru chains in the two electrodes. This makes the bulk Néel vectors of the electrodes aligned oppositely to the alignment of the interfacial moments. As a result, the large transmission of the AFMTJ for the P-aligned Néel vectors is reduced by the AP-aligned interfacial moments, while the low transmission of the AFMTJ for the AP-aligned Néel vectors is enhanced by the P-aligned interfacial moments, thus reducing the overall TMR. On the contrary, the interfacial RuO_2 layers are the same for an AFMTJ with an odd number of TiO_2 monolayers. As a result, the P (AP) state of the AFMTJ has P (AP) interfacial moments in the two electrodes. This matching enhances TMR. As evident from Fig. 6(c), the oscillatory TMR appears at different energies. It is slightly suppressed at high energy where TMR is large, while it is more pronounced at $E = -0.1$ eV where TMR has a minimum. These oscillations reflect the competition of bulk and interfacial contributions to TMR.

In order to further understand the influence of the interface structure on TMR, we replace the TiO_2 barrier in the AFMTJ with a vacuum layer of ~ 5 Å to construct a $RuO_2|\square|RuO_2$ (110) AFMTJ ($\square$ denotes the vacuum layer). We fix the left electrode and shift the right electrode to obtain different interface configurations, as shown in Fig. 7(a). The two interfaces in configuration (1) correspond to these in the $RuO_2/TiO_2/RuO_2$ (110) AFMTJ with an even number of TiO_2 monolayers, while the interfaces in configuration (2) represent these in the $RuO_2/TiO_2/RuO_2$ (110) with an odd number of TiO_2 monolayers. Configuration (3) is obtained by applying a quarter-unit-cell translation of the right electrode along the in-plane diagonal direction. Configuration (4) is obtained from configuration (3) by applying a half-unit-cell translation along the vertical direction in the right electrode. As seen from Fig. 7(b), TMR is significantly larger for configuration (2) than for configuration (1), which is expected due to the enhancement of TMR for configuration (2) and its reduction for configuration (1) by the interfacial magnetic moments [53]. On the other hand, a moderate TMR of the same magnitude is calculated for configurations (3) and (4). This is due to the misaligned horizontal Ru chains at the two interfaces, which averages out the interfacial effect on TMR [53].

Interface effects in AFMTJs are important due to interface roughness and disorder being inevitable in experimental conditions. In this regard, the previous predictions of large magnetoresistive effects in AFM spin valves [59–61] and AFMTJs [62–64] are not expected to be robust to interface roughness and disorder [65,66]. These predictions employed spin-degenerate AFM metals where the bulk contribution to TMR could not occur. The predicted large effects entirely relied on perfect interfaces and switching the interfacial magnetic moments between parallel- and antiparallel-like in conventional MTJs. In contrast, RuO_2 exhibits spin-dependent band structure which is largely responsible for TMR in $RuO_2/TiO_2/RuO_2$ (110) AFMTJs. While the interface magnetic structure contributes to TMR, its contribution is not dominant and therefore even in the presence of interface roughness the predicted large TMR effects are expected to survive. On the other hand, modern film-growth techniques are capable of fabricating high-quality epitaxial heterostructures with the atomic scale control of the interface structure. Using these techniques, it may be possible to manufacture $RuO_2/TiO_2/RuO_2$ (110) AFMTJs with a well-controlled interface structure and observe TMR oscillations predicted in this work.

The giant TMR effect in RuO_2 (110) based AFMTJs implies a possibility of a large STT in these junctions. However, since the longitudinal current in RuO_2 (110) is globally spin-polarized, the generated STT is expected to be mostly dampinglike [67–69]. This kind of STT is capable to drive an ultrafast oscillation of the Néel vector [70], but is not able to realize its deterministic switching. An accurate and efficient write-in may be realized by applying an in-plane current in the RuO_2 (110) free layer along the [001] direction. Such a current is globally spin-neutral, but staggered, i.e., it represents a Néel spin current [47]. For an AFMTJ with a nanoscale width and asymmetric boundary conditions, the Néel spin current can generate a net fieldlike STT for the deterministic switching of the RuO_2 free layer.

Furthermore, since antiferromagnets such as RuO_2 (110) host an unbalanced $p_\parallel(\vec{k}_\parallel)$, they could serve as counter electrodes in conventional MTJs with a single FM electrode, where the matching of the unbalanced $p_\parallel(\vec{k}_\parallel)$ in AFM and FM electrodes generates TMR [71–73]. It is interesting both from the fundamental point of view and from the practical perspective, as it allows using a spin-polarized current from an AFM electrode to generate STT on an FM electrode for magnetization switching and eliminates the pinning layer required in conventional MTJs.

IV. SUMMARY

In summary, we have investigated spin-polarized transport properties of $RuO_2/TiO_2/RuO_2$ (110) AFMTJs using first-principles quantum-transport calculations. We predicted a giant TMR effect in these junctions and showed that it is robust to the change of electron energy, barrier layer thickness, and the interface termination. The predicted TMR effect cannot be explained by the conventional picture based on the globally spin-polarized current produced by the RuO_2 (110) antiferromagnet but rather originates from the matching of the spin-polarized conduction channels in the two RuO_2 (110) electrodes. We found TMR oscillations with the increase of TiO_2 barrier thickness that reflect a non-negligible contribution from the perfectly epitaxial interfaces. Our work helps the understanding of the physics of TMR and aids in realizing functional AFMTJs in practice.

ACKNOWLEDGMENTS

This work was supported by the National Key Research and Development Program of China (Grants No. 2021YFA1600200 and No. 2022YFA1403203), the National Science Foundation of China (NSFC Grants No. 12241405, No. 12274411, No. 52250418, No. 12174019, No. 12274412, No. 12204009, and No. U2032215), the Basic Research Program of the Chinese Academy of Sciences Based on Major Scientific Infrastructures (Grant No. JZHKYPT-2021–08), and the CAS Project for Young Scientists in Basic Research (Project No. YSBR-084). Research at the University of Nebraska-Lincoln was supported by the Division of Materials Research of the National Science Foundation (NSF Grant No. DMR-2316665). The calculations were performed at the Hefei Advanced Computing Center.

[1] *Spintronics Handbook: Spin Transport and Magnetism*, 2nd ed., edited by E. Y. Tsymbal and I. Žutić (CRC, Boca Raton, FL, 2019).

[2] M. Julliere, Tunneling between ferromagnetic films, Phys. Lett. A **54**, 225 (1975).

[3] R. Meservey and P. M. Tedrow, Spin-polarized electron tunneling, Phys. Rep. **238**, 173 (1994).

[4] J. S. Moodera, L. R. Kinder, T. M. Wong, and R. Meservey, Large magnetoresistance at room temperature in ferromagnetic thin film tunnel junctions, Phys. Rev. Lett. **74**, 3273 (1995).

[5] E. Y. Tsymbal, O. N. Mryasov, and P. R. LeClair, Spin-dependent tunneling in magnetic tunnel junctions, J. Phys.: Condens. Matter **15**, R109 (2003).

[6] S. Yuasa, T. Nagahama, A. Fukushima, Y. Suzuki, and K. Ando, Giant room-temperature magnetoresistance in single-crystal Fe/MgO/Fe magnetic tunnel junctions, Nat. Mater. **3**, 868 (2004).

[7] S. Parkin, C. Kaiser, A. Panchula, P. M. Rice, B. Hughes, M. Samant, and S. H. Yang, Giant tunnelling magnetoresistance at room temperature with MgO (100) tunnel barriers, Nat. Mater. **3**, 862 (2004).

[8] A. V. Khvalkovskiy, D. Apalkov, S. Watts, R. Chepulskii, R. S. Beach, A. Ong, X. Tang, A. Driskill-Smith, W. H. Butler, P. B.Visscher, D. Lottis, E. Chen, V. Nikitin, and M. Krounbi, Basic principles of STT-MRAM cell operation in memory arrays, J. Phys. D **46**, 074001 (2013).

[9] Ph. Mavropoulos, N. Papanikolaou, and P. H. Dederichs, Complex band structure and tunneling through ferromagnet/insulator/ferromagnet junctions, Phys. Rev. Lett. **85**, 1088 (2000).

[10] W. H. Butler, X. G. Zhang, T. C. Schulthess, and J. M. MacLaren, Spin-dependent tunneling conductance of Fe|MgO|Fe sandwiches, Phys. Rev. B **63**, 054416 (2001).

[11] J. Mathon and A. Umerski, Theory of tunneling magnetoresistance of an epitaxial Fe/MgO/Fe (001) junction, Phys. Rev. B **63**, 220403(R) (2001).

[12] D.-F. Shao, S. H. Zhang, M. Li, C. B. Eom, and E. Y. Tsymbal, Spin-neutral currents for spintronics, Nat. Commun. **12**, 7061 (2021).

[13] L. Šmejkal, A. Birk Hellenes, R. González-Hernández, J. Sinova, and T. Jungwirth, Giant and tunneling magnetoresistance in unconventional collinear antiferromagnets with nonrelativistic spin-momentum coupling, Phys. Rev. X **12**, 011028 (2022).

[14] J. Dong, X. Li, G. Gurung, M. Zhu, P. Zhang, F. Zheng, E. Y. Tsymbal, and J. Zhang, Tunneling magnetoresistance in noncollinear antiferromagnetic tunnel junctions, Phys. Rev. Lett. **128**, 197201 (2022).

[15] G. Gurung, D.-F. Shao, and E. Y. Tsymbal, Extraordinary tunneling magnetoresistance in antiferromagnetic tunnel junctions with antiperovskite electrodes, arXiv:2306.03026.

[16] P. Qin, H. Yan, X. Wang, H. Chen, Z. Meng, J. Dong, M. Zhu, J. Cai, Z. Feng, X. Zhou, L. Liu, T. Zhang, Z. Zeng, J. Zhang, C. Jiang, and Z. Liu, Room-temperature magnetoresistance in an all-antiferromagnetic tunnel junction, Nature (London) **613**, 485 (2023).

[17] X. Chen, T. Higo, K. Tanaka, T. Nomoto, H. Tsai, H. Idzuchi, M. Shiga, S. Sakamoto, R. Ando, H. Kosaki, T. Matsuo, D. Nishio-Hamane, R. Arita, S. Miwa, and S. Nakatsuji, Octupole-driven magnetoresistance in an antiferromagnetic tunnel junction, Nature (London) **613**, 490 (2023).

[18] V. Baltz, A. Manchon, M. Tsoi, T. Moriyama, T. Ono, and Y. Tserkovnyak, Antiferromagnetic spintronics, Rev. Mod. Phys. **90**, 015005 (2018).

[19] T. Jungwirth, X. Marti, P. Wadley, and J. Wunderlich, Antiferromagnetic spintronics, Nat. Nanotechnol. **11**, 231 (2016).

[20] T. Berlijn, P. C. Snijders, O. Delaire, H.-D. Zhou, T. A. Maier, H.-B. Cao, S.-X. Chi, M. Matsuda, Y. Wang, M. R. Koehler, P. R. C. Kent, and H. H. Weitering, Itinerant antiferromagnetism in RuO_2, Phys. Rev. Lett. **118**, 077201 (2017).

[21] K.-H. Ahn, A. Hariki, K.-W. Lee, and J. Kuneš, RuO_2 antiferromagnetism in as *d*-wave pomeranchuk instability, Phys. Rev. B **99**, 184432 (2019).

[22] J. Železný, Y. Zhang, C. Felser, and B. Yan, Spin-polarized current in noncollinear antiferromagnets, Phys. Rev. Lett. **119**, 187204 (2017).

[23] G. Gurung, D.-F. Shao, and E. Y. Tsymbal, Transport spin polarization of noncollinear antiferromagnetic antiperovskites, Phys. Rev. Mater. **5**, 124411 (2021).

[24] S. Hayami, Y. Yanagi, and H. Kusunose, Momentum-dependent spin splitting by collinear antiferromagnetic ordering, J. Phys. Soc. Jpn. **88**, 123702 (2019).

[25] L.-D. Yuan, Z. Wang, J.-W. Luo, E. I. Rashba, and A. Zunger, Giant momentum-dependent spin splitting in centrosymmetric low-Z antiferromagnets, Phys. Rev. B **102**, 014422 (2020).

[26] L.-D. Yuan, Z. Wang, J.-W. Luo, and A. Zunger, Prediction of low-Z collinear and noncollinear antiferromagnetic compounds having momentum-dependent spin splitting even without spin-orbit coupling, Phys. Rev. Mater. **5**, 014409 (2021).

[27] M. Naka, S. Hayami, H. Kusunose, Y. Yanagi, Y. Motome, and H. Seo, Spin current generation in organic antiferromagnets, Nat. Commun. **10**, 4305 (2019).

[28] R. González-Hernández, L. Šmejkal, K. Výborný, Y. Yahagi, J. Sinova, T. Jungwirth, and J. Železný, Efficient electrical spin-splitter based on non-relativistic collinear antiferromagnetism, Phys. Rev. Lett. **126**, 127701 (2021).

[29] L. Šmejkal, J. Sinova, and T. Jungwirth, Beyond conventional ferromagnetism and antiferromagnetism: A phase with nonrelativistic spin and crystal rotation symmetry, Phys. Rev. X **12**, 031042 (2022).

[30] L. Šmejkal, J. Sinova, and T. Jungwirth, Emerging research landscape of altermagnetism, Phys. Rev. X **12**, 040501 (2022).

[31] H. Bai, L. Han, X. Y. Feng, Y. J. Zhou, R. X. Su, Q. Wang, L. Y. Liao, W. X. Zhu, X. Z. Chen, F. Pan, X. L. Fan, and C. Song, Observation of spin splitting torque in a collinear antiferromagnet RuO_2, Phys. Rev. Lett. **128**, 197202 (2022).

[32] P. Hohenberg and W. Kohn, Inhomogeneous electron gas, Phys. Rev. **136**, B864 (1964).

[33] G. Kresse and J. Hafner, *Ab initio* molecular dynamics for liquid metals, Phys. Rev. B **47**, 558 (1993).

[34] G. Kresse and J. Furthmuller, Efficient iterative schemes for *ab initio* total-energy calculations using a plane-wave basis set, Phys. Rev. B **54**, 11169 (1996).

[35] G. Kresse and D. Joubert, From ultrasoft pseudopotentials to the projector augmented-wave method, Phys. Rev. B **59**, 1758 (1999).

[36] J. P. Perdew, K. Burke, and M. Ernzerhof, Generalized gradient approximation made simple, Phys. Rev. Lett. **77**, 3865 (1996).

[37] V. V. Anisimov, J. Zaanen, and O. K. Andersen, Band theory and mott insulators: Hubbard U instead of stoner I, Phys. Rev. B **44**, 943 (1991).

[38] S. L. Dudarev, G. A. Botton, S. Y. Savrasov, C. J. Humphreys, and A. P. Sutton, Electron-energy-loss spectra and the structural stability of nickel oxide: An LSDA+U study, Phys. Rev. B **57**, 1505 (1998).

[39] A. A. Mostofi, J. R. Yates, G. Pizzi, Y. S. Lee, I. Souza, D. Vanderbilt, and N. Marzari, An updated version of wannier90: A tool for obtaining maximally-localised Wannier functions, Comput. Phys. Commun. **185**, 2309 (2014).

[40] N. Marzari and D. Vanderbilt, Maximally localized generalized Wannier functions for composite energy bands, Phys. Rev. B **56**, 12847 (1997).

[41] I. Souza, N. Marzari, and D. Vanderbilt, Maximally localized Wannier functions for entangled energy bands, Phys. Rev. B **65**, 035109 (2001).

[42] M. Kawamura, FermiSurfer: Fermi-surface viewer providing multiple representation schemes, Comput. Phys. Commun. **239**, 197 (2019).

[43] J. Taylor, H. Guo, and J. Wang, *Ab initio* modeling of quantum transport properties of molecular electronic devices, Phys. Rev. B **63**, 245407 (2001).

[44] M. Brandbyge, J.-L. Mozos, P. Ordejón, J. Taylor, and K. Stokbro, Density-functional method for nonequilibrium electron transport, Phys. Rev. B **65**, 165401 (2002).

[45] S. Smidstrup, T. Markussen, P. Vancraeyveld *et al.*, QuantumATK: An integrated platform of electronic and atomic-scale modelling tools, J. Phys.: Condens. Matter **32**, 015901 (2020).

[46] D. R. Hamann, Optimized norm-conserving Vanderbilt pseudopotentials, Phys. Rev. B **88**, 085117 (2013).

[47] D. F. Shao, Y. Y. Jiang, J. Ding, S. H. Zhang, Z. A. Wang, R. C. Xiao, G. Gurung, W. J. Lu, Y. P. Sun, and E. Y. Tsymbal, Néel spin currents in antiferromagnets, Phys. Rev. Lett. **130**, 216702 (2023).

[48] A. Bose, N. J. Schreiber, R. Jain, D.-F. Shao, H. P. Nair, J. Sun, X. S. Zhang, D. A. Muller, E. Y. Tsymbal, D. G. Schlom, and D. C. Ralph, Tilted spin current generated by the collinear antiferromagnet ruthenium dioxide, Nat. Electron. **5**, 267 (2022).

[49] D.-F. Shao, S.-H. Zhang, R.-C. Xiao, Z.-A. Wang, W. J. Lu, Y. P. Sun, and E. Y. Tsymbal, Spin-neutral tunneling anomalous hall effect, Phys. Rev. B **106**, L180404 (2022).

[50] S. Karube, T. Tanaka, D. Sugawara, N. Kadoguchi, M. Kohda, and J. Nitta, Observation of spin-splitter torque in collinear antiferromagnetic RuO_2, Phys. Rev. Lett. **129**, 137201 (2022).

[51] L. Šmejkal, R. González-Hernández, T. Jungwirth, and J. Sinova, Crystal hall effect in collinear antiferromagnets, Sci. Adv. **6**, eaaz8809 (2020).

[52] Z. Feng, X. Zhou, L. Šmejkal, L. Wu, Z. Zhu, H. Guo, R. González-Hernández, X. Wang, H. Yan, P. Qin, X. Zhang, H. Wu, H. Chen, C. Jiang, M. Coey, J. Sinova, T. Jungwirth, and Z. Liu, An anomalous Hall effect in altermagnetic ruthenium dioxide, Nat. Electron. **5**, 735 (2022).

[53] See Supplemental Material at http://link.aps.org/supplemental/10.1103/PhysRevB.108.174439 for the electronic structure of bulk RuO_2 (110), the density of states (DOS) of the $RuO_2/TiO_2/RuO_2$ (110) AFMTJ, the transmission in $RuO_2/TiO_2/RuO_2$ (110) AFMTJ with different TiO_2 thickness, and the transmission in $RuO_2/\square/RuO_2$ (110) AFMTJ with different atomic configurations.

[54] R. J. Soulen, Jr., J. M. Byers, M. S. Osofsky, B. Nadgorny, T. Ambrose, S. F. Cheng, P. R. Broussard, C. T. Tanaka, J. Nowak, J. S. Moodera, A. Barry, and J. M. D. Coey, Measuring the spin polarization of a metal with a superconducting point contact, Science **282**, 85 (1998).

[55] S. K. Upadhyay, A. Palanisami, R. N. Louie, and R. A. Buhrman, Probing ferromagnets with Andreev reflection, Phys. Rev. Lett. **81**, 3247 (1998).

[56] I. I. Mazin, How to define and calculate the degree of spin polarization in ferromagnets, Phys. Rev. Lett. **83**, 1427 (1999).

[57] K. D. Belashchenko, E. Y. Tsymbal, M. van Schilfgaarde, D. Stewart, I. I. Oleinik, and S. S. Jaswal, Effect of interface bonding on spin-dependent tunneling from the oxidized Co surface, Phys. Rev. B **69**, 174408 (2004).

[58] K. D. Belashchenko and E. Y. Tsymbal, Tunneling magnetoresistance: Theory, in *Spintronics Handbook: Spin Transport and Magnetism*, 2nd ed., edited by E. Y. Tsymbal and I. Žutić (CRC, Boca Raton, FL, 2019), p. 525.

[59] A. S. Núñez, R. A. Duine, P. Haney, and A. H. MacDonald, Theory of spin torques and giant magnetoresistance

in antiferromagnetic metals, Phys. Rev. B **73**, 214426 (2006).

[60] P. M. Haney, D. Waldron, R. A. Duine, A. S. Núñez, H. Guo, and A. H. MacDonald, *Ab initio* giant magnetoresistance and current-induced torques in Cr/Au/Cr multilayers, Phys. Rev. B **75**, 174428 (2007).

[61] Y. Xu, S. Wang, and K. Xia, Spin-transfer torques in antiferromagnetic metals from first principles, Phys. Rev. Lett. **100**, 226602 (2008).

[62] P. Merodio, A. Kalitsov, H. Ba, V. Baltz, and M. Chshiev, Spin-dependent transport in antiferromagnetic tunnel junctions, Appl. Phys. Lett. **105**, 122403 (2014).

[63] M. Stamenova, R. Mohebbi, J. Seyed-Yazdi, I. Rungger, and S. Sanvito, First-principles spin-transfer torque in CuMnA|GaP|CuMnAs junctions, Phys. Rev. B **95**, 060403(R) (2017).

[64] H. Saidaoui, A. Manchon, and X. Waintal, Robust spin transfer torque in antiferromagnetic tunnel junctions, Phys. Rev. B **95**, 134424 (2017).

[65] H. B. M. Saidaoui, A. Manchon, and X. Waintal, Spin transfer torque in antiferromagnetic spin valves: From clean to disordered regimes, Phys. Rev. B **89**, 174430 (2014).

[66] A. Manchon, Spin diffusion and torques in disordered antiferromagnets, J. Phys.: Condens. Matter **29**, 104002 (2017).

[67] O. V. Gomonay and V. M. Loktev, Spin transfer and current-induced switching in antiferromagnets, Phys. Rev. B **81**, 144427 (2010).

[68] R. Cheng, M. W. Daniels, J.-G. Zhu, and D. Xiao, Ultrafast switching of antiferromagnets via spin-transfer torque, Phys. Rev. B **91**, 064423 (2015).

[69] O. Gomonay, V. Baltz, A. Brataas, and Y. Tserkovnyak, Antiferromagnetic spin textures and dynamics, Nat. Phys. **14**, 213 (2018).

[70] R. Cheng, D. Xiao, and A. Brataas, Terahertz antiferromagnetic spin hall nano-oscillator, Phys. Rev. Lett. **116**, 207603 (2016).

[71] K. Samanta, D.-F. Shao, T. R. Paudel, and E. Y. Tsymbal, Giant tunneling magnetoresistance in magnetic tunnel junctions with a single ferromagnetic electrode, in *Abstracts of the 68th Annual MMM Conference* (AIP Publishing, Dallas, Texas, 2023), p. 206.

[72] K. Samanta, Y.-Y. Jiang, T. R. Paudel, D.-F. Shao, and E. Y. Tsymbal, Tunneling magnetoresistance in magnetic tunnel junctions with a single ferromagnetic electrode, arXiv:2310.02139.

[73] B. Chi, L. Jiang, Y. Zhu, G. Yu, C. Wan, J. Zhang, and X. Han, Altermagnetic tunnel junctions of $RuO_2/TiO_2/CrO_2$, arXiv:2309.09561.